0191-8141/98 $19.00 + 0.00

Prediction of faulting from the theories of elasticity and plasticity: what are the limits?

MURIEL GERBAULT, ALEXEI N. B. POLIAKOV and MARC DAIGNIERES

Laboratoire de Géophysique et Tectonique (U.M.R. 5573), CNRS-Université Montpellier II, 34095 Montpellier 05, France

Abstract—Elasticity, rigid-plasticity and elasto-plasticity are the simplest constitutive models used to describe the initiation and evolution of faulting. However, in practice, the limits of their application are not always clear. In this paper, we test the behaviour of these different models using as examples tectonic problems of indentation of a die, compression with basal shear, bending of a plate and normal faulting around a dike. By comparing the results of these tests, we formulate some guidelines that may be useful for the selection of an appropriate constitutive model of faulting. The theory of elasticity reasonably predicts the initiation of the fault pattern but gives erroneous results for large strains. The theory of rigid-plasticity is more appropriate for large deformations, where the geometry of faults can be found by the method of characteristics. This method works well for zones of failure that are not severely constrained by elastic material outside, e.g. when faults are connected to the free-surface, a viscous substratum or a zone of weakness. Non-associated elasto-plasticity is the most complete theory among those considered in this paper. It describes the evolution of faults from the initiation of localized deformations to the formation of a complicated fault network.

INTRODUCTION

It is important for geologists to have a simple constitutive model that describes the initiation and evolution of faulting. The field of mechanics offers some idealized models for the behaviour of materials during faulting such as elasticity, rigid-plasticity and elasto-plasticity. These theories are widely used, and sometimes misused, in structural geology. There is a need for a clear demonstration of the abilities and limitations of these constitutive models in order to develop intuition about fault prediction. Progress in this field can be made by modelling of simple, idealized tectonic situations such as thrusting, bending or indentation by means of each theory.

There are several mechanical approaches to the prediction of the location and geometry of faults. The simplest way is to calculate the stress field in the region of interest by means of the theory of elasticity (Anderson, 1951; Hafner, 1951; Sanford, 1959; Spencer and Chase, 1989; Yin, 1989; Parsons and Thompson, 1993). The faults are predicted to be at a certain angle from the direction of principal stresses where the condition for fault friction is satisfied. This simple approach may give correct first-order predictions for fault initiation. However, when it is not used carefully, it gives unreasonable results (Buck, 1990; Wills and Buck, 1997). Furthermore, the weakness of this method is that faulting changes the predicted elastic state, and this theory does not take into account the conditions necessary for fault slippage.

A more advanced approach involves the use of different theories of plasticity. The classical 'metal' rigid-plasticity, which can be treated analytically in many cases, provides a stress distribution that satisfies the failure criterion and the kinematically admissible velocity field, where faults can be interpreted as velocity discontinuities (Odé, 1960). This approach was used for fault prediction in thrusts and accretionary prisms (Stockmal, 1983; Dahlen, 1984), for rifting (Lin and Parmentier, 1990) and continent collision (Tapponnier and Molnar, 1976; Regenauer-Lieb, 1996; Regenauer-Lieb and Petit, 1997). One of the drawbacks of this method is the uncertainty in the choice of the geometry of the failure zone, due to the assumption that the material outside the plastic zone is rigid. The other problem is that the kinematics of faulting in pressure-dependent rocks is unrealistic.

The theory of elasto-plasticity with realistic kinematics of failure (so-called 'non-associated' flow rule) is the most appropriate theory for faulting. It has taken a long time for non-associated plasticity to be developed and accepted in mechanics (Mandel, 1966; Salençon, 1974; Rudnicki and Rice, 1975; Mandl *et al.*, 1977; Vermeer and de Borst, 1984; Vardoulakis and Salem, 1995). Analytical solutions are available only for simple cases such as a single shear band (Vermeer, 1990; Byerlee and Savage, 1992), whereas geological problems require direct numerical simulation (Hobbs and Ord, 1989; Cundall, 1990; Hobbs *et al.*, 1990; Poliakov *et al.*, 1994; Poliakov and Herrmann, 1994; Hassani and Chéry, 1996; Hassani *et al.*, 1996; Leroy and Triantafyllidis, 1996).

This paper tries to demonstrate that the selection of the appropriate constitutive behaviour depends on whether one needs to describe the initiation of faulting, the approximate geometry of the failure zone or the evolution of individual faults in time. The first part of the paper is devoted to a review of the theory, considering the extent to which faulting can be predicted by the theories of elasticity, 'associated' rigid-plasticity and 'non-associated' elasto-plasticity. Each approach is illustrated with the example of an indenter (flat die) penetrating into a half-space. The second part of the paper treats the

seemingly simple cases of compression with basal shear, bending and faulting around a dike. Based on the experience gained from these cases, some simple rules of thumb for fault prediction are provided, and the limitations of each approach are discussed in the third part. This study is meant to be a demonstration of the applicability of the theory of elasto-plasticity for the geological community, and an introduction to some geological problems for mechanicists.

THEORETICAL BACKGROUND WITH AN EXAMPLE OF INDENTATION IN A HALF-SPACE

Andersonian and elasticity theories

A great advance in the application of basic mechanics to geological problems was accomplished by Anderson (1951). He made two assumptions about the initiation of faults in the earth. First, he proposed that faults form and slip on planes which are oriented at $45^\circ - \phi/2^\circ$ to the maximum compressive stress (Fig. 1). The shear stress τ thus satisfies the Mohr–Coulomb criterion:

$$\tau = -\tan(\phi) \cdot \sigma_n + C, \qquad (1)$$

where ϕ is the angle of friction, σ_n is the normal stress acting on the plane, and C is the cohesion.

Second, he assumed that all the principal stresses are either horizontal or vertical. This theory predicts the three types of observed faults, thrust, strike-slip and normal fault, depending on which of the principal stresses is vertical. Andersonian predictions of the orientation of each type of fault are consistent with many observations (e.g. Sibson, 1994).

Following the ideas of Anderson, many people tried to apply the Mohr–Coulomb fracture criterion to more complex stress fields to investigate the evolution of fault geometries for large displacements. One 'classical' approach has been to calculate lithospheric stress fields due to topographic or other loads from elasticity theory, and then assume that faults are oriented at the angle $\pm(45^\circ - \phi/2)$ to the most compressive stress. This idea

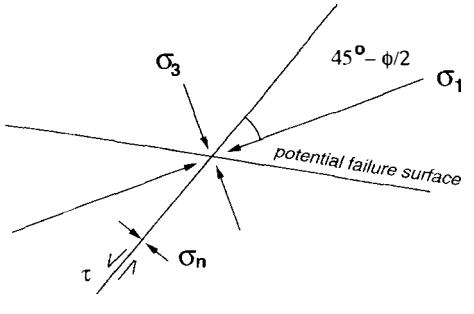

Fig. 1. Prediction of faulting in an elastic material. Potential planes of failure are oriented at $\pm(45^\circ - \phi/2)$ to the maximum pressive stress, σ_1, for which equation (1) is satisfied.

was applied to the prediction of faulting due to compression with a basal shear (Hafner, 1951; Yin, 1989, 1993), flexure of the crust (Sanford, 1959; Spencer and Chase, 1989) and magmatism in extensional stress field (Parsons and Thompson, 1993). Some of these solutions will be shown in the next part of the paper. Criticism of the use of this approach for certain cases is provided by Buck (1990) and Wills and Buck (1997).

Pros and cons of the 'elastic' approach. This method of fault prediction is appealing for the following reasons:

(1) It is consistent with observations of the fault orientations at large tectonic scales (e.g. Sibson, 1994).

(2) Elastic analytical solutions are relatively simple and intuitive. They are useful for a crude estimation of where faults can appear.

(3) This method should predict fairly well the initial failure zones that can persist during large deformations, if fault strength rapidly degrades.

However, there are several reasons for why the results from these models may be misleading.

(1) As soon as material reaches a critical state (failure) and faults develop in one area, the stress distribution is changed from the subcritical state predicted from elasticity theory.

(2) This approach completely ignores the kinematics of the problem. The predicted direction of failure planes may be incompatible with the boundary conditions.

(3) Even if the slip along the surface of initial failure is kinematically admissible, it may require more energy to slip along the 'Andersonian' fault than along the other fault orientations, which are not favored initially (Buck, 1992; Forsyth, 1992).

Because it is not possible to resolve these issues for the general case, we have found it constructive to focus on concrete examples of fault initiation. As a benchmark, we have chosen the problem of indentation of a flat die in the half-space, because analytical solutions for elastic and plastic material are available, and this problem is numerically tractable.

Indentation in the half-space. Consider the example of a frictionless die pushed into an elastic half-space (Fig. 2a). The distribution of stresses can be found analytically for the case in which the die is replaced by a strip of normal stress at the top of the domain (Crouch and Starfield, 1990). The contours of maximum shear stresses form crescents that terminate at the corners of the die, and may represent the boundary between intact and failed material. The region where the limiting stress is above 3 MPa is shown, together with potential trajectories of failure planes, for an indentation load $q = 15$ MPa.

Theory of rigid-plasticity

Plasticity theory is a more suitable approach for

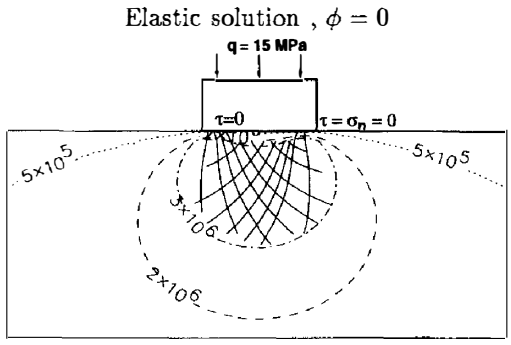

a)

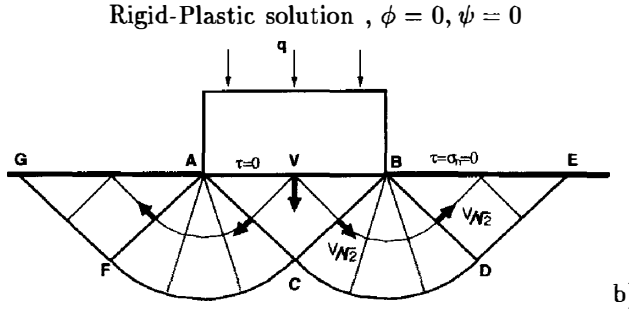

b)

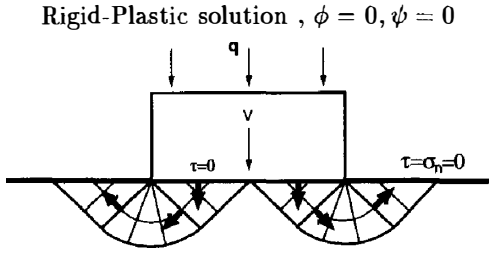

c)

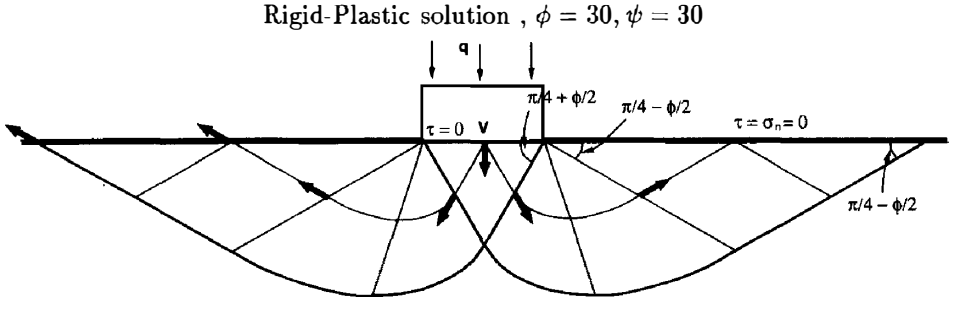

d)

Fig. 2. Failure zones due to vertical stress q applied to elastic (a) and rigid-plastic (b–d) half-space. (a) Trajectories of potential failure are shown as solid lines inside the domain where the maximum shearing stress k is above 3 MPa. (b) Prantdl's solutions for slip-lines in a rigid-plastic material with pressure-independent yield criterion ($\phi = 0$). The limit stress q is $(\pi + 2)k$. (c) Alternative Hill's solution illustrates the non-uniqueness of plastic zone configuration for the same limiting stress. (d) Slip-lines in a pressure-dependent rigid-plastic material with friction angle and dilatancy $\phi = \psi = 30°$, where limiting q is $\approx 30C$, and C is cohesion.

prediction of faulting because it takes into account limiting (yield) stress and defines 'slip-lines', which can be interpreted as tectonic faults (Odé, 1960).

Here, we briefly discuss two main points concerning basic rigid-plasticity (Hill, 1950; Johnson *et al.*, 1970; Backhofen, 1972; Johnson and Mellor, 1983). First, due to the complexity of solutions for elasto-plastic rheology, material is assumed to be rigid-plastic, or elasto-plastic with an infinite elastic modulus. Although this assumption may be justified if elastic strains that are small compared to plastic ones are disregarded, it may produce serious errors for certain problems. Secondly, the distribution of stresses in rigid zones is not determined, nor is the boundary between plastic and rigid zones, which should be at the yield stress.

Thus, the configuration of plastic zones, and stress and velocity fields are non-unique and need to be chosen before the problem can be solved. The choice of plastic zones is somewhat arbitrary, but should satisfy certain criteria (described below). When the configurations of the plastic zone are chosen, the stress distribution and velocity field in this zone can be found.

The rheology of rocks can be classified into those where the yield stresses depend on pressure and those where they do not. The theory of plasticity can be applied for either case. We start with the case of pressure-independent plasticity. The plane-strain approximation is used for all problems considered below.

Pressure-independent plasticity. Plastic material yields when the maximum shear stress, τ, reaches a critical value, k, which is a material constant,

$$\tau^2 = -\frac{1}{4}(\sigma_{xx} - \sigma_{yy})^2 + \tau_{xy}^2 = k^2, \tag{2}$$

where σ_{xx}, σ_{yy}, τ_{xy} are the components of the Cauchy stress tensor. The yield stress is assumed to be independent of pressure, and does not change with strain (perfect plasticity). The yield surface in stress space (σ_n, τ) is shown in Fig. 3(a), and is the same for Tresca and Von Mises materials in plane strain problems.

The set of two equations of equilibrium in the absence of body forces reduces to

$$\frac{\partial \sigma_{xx}}{\partial x} + \frac{\partial \tau_{xy}}{\partial y} = 0 \qquad \frac{\partial \sigma_{yy}}{\partial y} + \frac{\partial \tau_{xy}}{\partial x} = 0. \tag{3}$$

Equations (2) and (3) give a system of three equations with three unknowns σ_{xx}, σ_{yy}, τ_{xy}. If the boundary conditions involve only stresses, such a problem is statically determined; velocities can be found afterwards.

Plastic flow is assumed to be incompressible,

$$\frac{\partial v_x}{\partial x} + \frac{\partial v_y}{\partial y} = 0, \tag{4}$$

where v_x and v_y are components of the velocity vector. In an isotropic material, the direction of the principal axes of stress and plastic strain-rate must coincide (hypothesis of Saint-Venant); thus

$$\tan 2(\widehat{x, \sigma_1}) = \frac{2\sigma_{xy}}{\sigma_{xx} - \sigma_{yy}} = \frac{2\dot{\varepsilon}^p_{xy}}{\dot{\varepsilon}^p_{xx} - \dot{\varepsilon}^p_{yy}} = \frac{\left(\frac{\partial v_x}{\partial y} + \frac{\partial v_y}{\partial x}\right)}{\left(\frac{\partial v_x}{\partial x} - \frac{\partial v_y}{\partial y}\right)}, \tag{5}$$

where $(\widehat{x, \sigma_1})$ is the angle between the X axis and direction of σ_1 Fig. 3(b), and $\dot{\varepsilon}^p_{xy}$, $\dot{\varepsilon}^p_{xx}$, $\dot{\varepsilon}^p_{yy}$ are the components of plastic strain rate tensor. If the distribution of stresses is known, then velocities v_x and v_y can be found from equations (4) and (5).

The condition of coaxiality between strain-rate and stress tensors can be also written as the proportionality between deviatoric stress s_{ij} and plastic strain-rate $\dot{\varepsilon}^p_{ij}$,

$$\dot{\varepsilon}^p_{ij} = \lambda s_{ij} \quad s_{ij} = \sigma_{ij} + p\delta_{ij} \tag{6}$$

where λ is the coefficient of the proportionality and pressure is $p = -(\sigma_{xx} + \sigma_{yy})/2$ for the plane strain problem. The relation (6) is shown graphically in Fig. 3(a). The intersection of the yield stress envelope and Mohr circle determines the direction of the plane of failure. One can define the stress acting on this plane as a vector in the (σ_n, τ) space. We plot the vector of deviatoric stress $\vec{s}$ which is orthogonal to the yield surface. The vector of plastic strain rate $\dot{\vec{\varepsilon}}_p$ can be plotted parallel to the $\vec{s}$ because of the coaxiality of plastic strain rate and stress (equation (5)).

It can be seen in Fig. 3(a) that the plastic strain vector is orthogonal to the yield surface. The condition of the orthogonality, or associativity, is also the consequence of the fundamental 'maximum work' principle in the theory of metal plasticity (Hill, 1950).

The maximum shear stress and strain rates are oriented at 45° to the axes of principal stresses, forming an angle θ with the X axis (Fig. 3b). These are called slip-lines because slip can occur only along these directions. They form two orthogonal families of curves shown as α and β lines in Fig. 3(c).

It can be shown (Hill, 1950) that the system of equations (2) and (3) exhibits the fundamental property that, along the slip-lines, certain quantities are conserved:

$$\begin{aligned} p + 2k\theta &= \text{const on an } \alpha \text{ line} \\ p - 2k\theta &= \text{const on a } \beta \text{ line,} \end{aligned} \tag{7}$$

where k is maximum shear stress and p is the pressure (Fig. 3c). These relations are called the Hencky equations. It also can be shown that equation (2) with condition (3) is hyperbolic, and the characteristic curves are the slip lines (Hill, 1950). The solution of a given rigid-plastic problem requires construction of the slip-line field. These can be found by propagation from the boundary where stresses are defined. Although, in a general case, it is required to be done numerically, for some cases, it can be done analytically. For example, if the boundary is straight and shear stresses at the

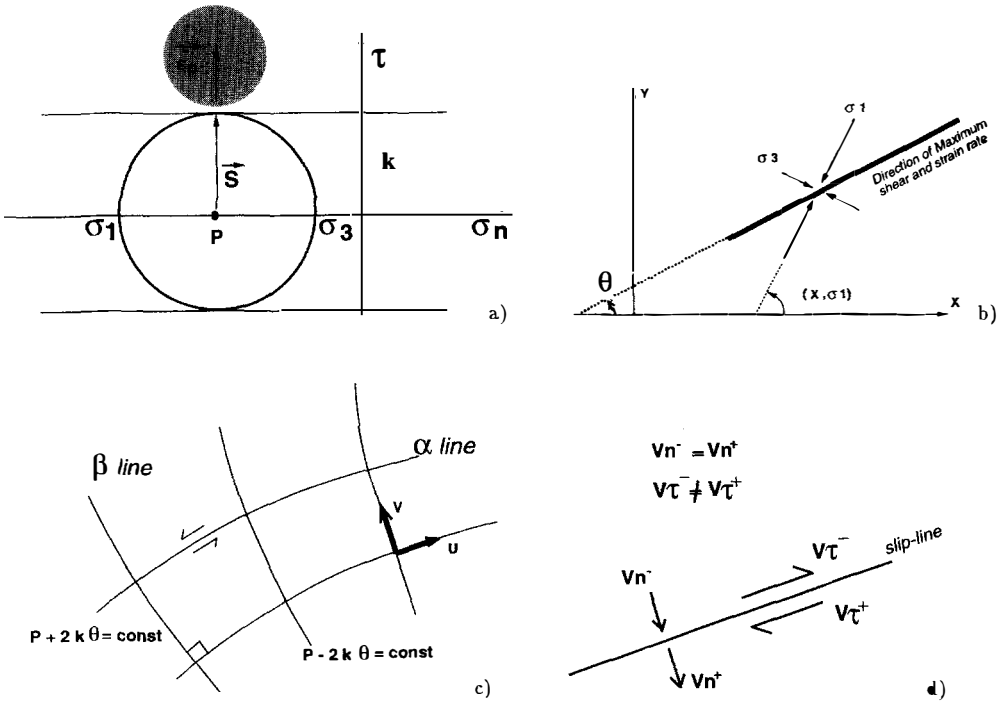

Fig. 3. (a) Limiting (yield) stress for pressure-independent material with incompressible plastic flow $\phi = \psi = 0$ in the (τ, σ_n) stress space. Plastic strain rate $\dot{\varepsilon}_p$ is shown inside a grey circle because it is defined in another space. It is coaxial to the deviatoric shear stress $\vec{s}$ (equation (6)). (b) Direction of maximum shearing stress makes an angle θ to the x axis and 45° to σ_1. (c) Directions of maximum shear stress and strain form two sets of perpendicular α and β slip-lines along which equation (7) is satisfied. (d) Properties of velocity field: normal velocity is continuous across a slip-line, tangential velocity can be discontinuous and can be interpreted as a fault.

boundary are zero, then the adjacent plastic zone is a triangle where the slip-lines are straight lines.

The velocity field has a similar property as the stress such that

$$\mathrm{d}u - v\mathrm{d}\theta = 0 \text{ on an } \alpha \text{ line}$$
$$\mathrm{d}v + u\mathrm{d}\theta = 0 \text{ on a } \beta \text{ line},$$

where u and v are velocity along slip-lines (Fig. 3c). These equations are attributed to Geiringer. They are nothing more than the statement that the rate of extension along any slip-line is zero. A fundamental property of these equations is that velocity u can be discontinuous across the α line and velocity v discontinuous across the β line. In other words, the normal velocity is continuous across the slip-line, while the tangential velocity can be discontinuous (Fig. 3d). This discontinuity can be interpreted as a fault (Odé, 1960). The frontier between plastic and rigid zones also should be a slip-line, separating moving from motionless material.

Indentation problem and non-uniqueness of the solution. The classical example of rigid frictionless die indenting in a half-space can be readily solved by means of rigid-plasticity theory. Figure 2(b) shows the construction of slip-lines proposed by Prantdl. Suppose that distribution of stresses is uniform under the indenter. The surface of the half-space is flat and shear stresses are zero. Thus, slip-lines are straight, tilted at 45° to the surface and form three triangles AFG, ACB and BDE. Two curved domains (AFC and BCD) are bridging these triangles. The triangles BDE and AFG are under horizontal compression, and triangle ABC is under horizontal tension. The α slip-line makes an angle $\theta_1 = -\pi/4$ to the free-surface and equation (7) yields,

$$p_1 - \frac{k\pi}{2} = \xi = \text{const} = \xi_1,$$

where p_1 is the undetermined pressure inside ΔABC. In ΔBDE, the following relations

$$\theta_2 = \frac{\pi}{4},\ p_2 = k,\ p_2 + \frac{k\pi}{2} = \xi_2$$

are satisfied along the same α slip-line. As the parameter ξ should be constant along an α line, $\xi_1 = \xi_2$ and the pressure under the die is $p_1 = k(\pi + 1)$. The difference between the pressure and vertical stress is k, and the limiting stress q applied to the die is

$$q = k(\pi + 2). \tag{8}$$

The kinematics of the plastic flow are simple: triangle ABC moves downwards, with velocity of the die V. The tangential component of velocity is discontinuous along line BC, while the normal component of velocity is continuous and is $V/\sqrt{(2)}$. Along CD, the tangential component of velocity is discontinuous, and the normal component is zero. The velocity in triangle BCD is $v = 0$ and $u = V/\sqrt{(2)}$. The domain BDE slips as a solid block in the direction DE at the same velocity, $V/\sqrt{(2)}$.

An alternative solution is that of Hill and is shown in

Fig. 2(c). One can also construct a number of slip-line fields which are a mixture of these two solutions. The limiting stress $q = k(\pi + 2)$ is the same for all these solutions.

The geometry of plastic zones is non-unique because the stress is not defined in rigid zones. Thus, it is necessary to make an additional verification of the solution by doing the following.

(1) Check that the velocity field is kinematically admissible, e.g. that slip-lines (or discontinuity line) do not terminate at a boundary with a rigid zone.

(2) Check that the dissipation of plastic flow $\sigma_{ij}\dot{\varepsilon}^p_{ij}$ is not negative.

(3) Choose the solution with the minimum limit load.

(4) Check that the stress in the rigid zones does not exceed the yield stress. This condition can be verified by propagation of plastic fields in the rigid zones.

However, these additional constraints may not be enough to distinguish between different solutions, as was the case for the solutions of Hill and Prantdl. A useful approach is to try to construct the geometry of the plastic zone by taking into account the theory of elasticity, or conduct a direct laboratory or numerical experiment, as will be shown below.

Mohr–Coulomb 'associated' plasticity. Pressure-dependent (Mohr–Coulomb) plasticity is more appropriate for the description of brittle failure in rocks and in soils. The yield stress envelope is shown in Fig. 4(a), where C is cohesion, ϕ is friction angle and $H = C\cdot\cot\phi$. The yield condition expressed in terms of principal stresses is

$$(\sigma_1 - \sigma_3) = -\sin(\phi)\cdot(\sigma_1 + \sigma_3 - 2H). \tag{9}$$

This is equivalent to equation (1). Equation (9) and the two equilibrium equations in equation (2) form a system of three equations with three unknowns as in the previous case.

The failure planes are inclined at $\pm(\pi/4 - \phi/2)$ angles to the direction of the principal stress σ_1 (Fig. 4b). These lines are also the slip-lines along which the following conditions are met (Salençon, 1974):

$$\begin{aligned} &\log(H+p) + \tan\phi\cdot 2\theta = \text{const on an } \alpha \text{ line} \\ &\log(H+p) - \tan\phi\cdot 2\theta = \text{const on a } \beta \text{ line.} \end{aligned} \tag{10}$$

As in the theory of pressure-independent plasticity, the principal directions of strain-rate and stresses are assumed to coincide. The plastic strain rate vector $\vec{\dot{\varepsilon}}_p$ is parallel to the deviatoric stress vector $\vec{s}$ (Fig. 4a). Thus, the plastic strain rate is associated with the yield surface. The relation between the shear $\dot{\varepsilon}^p_\tau$ and the volumetric $\dot{\varepsilon}^p_v$ components of the plastic strain rate at the plane of failure is,

$$\dot{\varepsilon}^p_v = \dot{\varepsilon}^p_\tau \tan(\phi), \tag{11}$$

where $\dot{\varepsilon}^p_v = 1/2(\dot{\varepsilon}^p_{xx} + \dot{\varepsilon}^p_{yy})$. Thus, the flow along the failure plane is not incompressible as was assumed in the analysis of pressure-independent plasticity, but increases in volume with an angle of dilatation ψ equal to the friction angle ϕ, where ψ is defined as $sin(\psi) = \dot{\varepsilon}^p_v/\dot{\varepsilon}^p_\tau$ (Vermeer and de Borst, 1984). This is the result of the 'associated' plastic flow rule and can cause serious problems in applications to real materials, because this condition is not physical.

Let us consider the problem of indentation in a pressure-dependent Coulomb material. Figure 2(d) shows that the construction of slip lines is similar to Prantdl's solution. However, the characteristics are oriented at $\pm(\pi/4 - \phi/2)$ to the maximum compressive stress. One can see that slip-lines initiate at the die with a slope of 60°, and terminate at the surface on the sides of the indenter at 30°. Using equation (10), we find the following relation for the limiting load q,

$$q = C\cot\phi\cdot\left(\frac{1+\sin\phi}{1-\sin\phi}e^{\pi\tan\phi} - 1\right). \tag{12}$$

Taking the value, $\phi = 30°$, we have $q \approx 30C$. This case will be verified numerically and compared with others in the next section.

Pros and cons of the rigid-plastic approach. The advantages of rigid-plasticity compared to elasticity are as follows.

(1) The stresses in the failure zones do not exceed the limit.

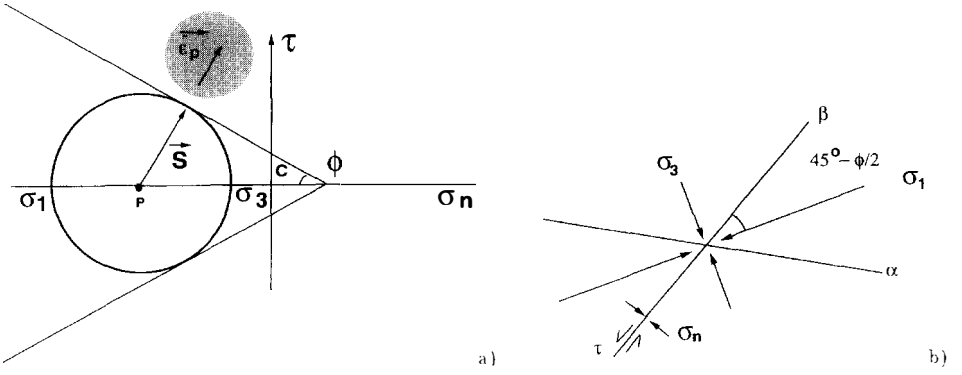

Fig. 4. (a) Yield stress for pressure-dependent (Coulomb) material with associated plastic flow $\phi = \psi = 30°$. Plastic strain rate $\vec{\dot{\varepsilon}}_p$ is coaxial to the deviatoric shear stress $\vec{s}$. (b) α and β slip-lines are oriented at $\pm(45 - \phi/2)$ to σ_1.

(2) The kinematics of failure are taken into account. Slip-lines can be interpreted as faults because the tangential velocities can be discontinuous across these lines. Thus, the theory of rigid-plasticity can predict movement for large deformation in contrast to the 'elastic' solution.

(3) In some cases, it is easier to construct the slip-line field or at least a part of it compared to the 'elastic' solutions, as in the problem of indentation.

The drawbacks of rigid-plasticity are the following.

(1) Non-uniqueness of the plastic zone configurations occur because the stress in rigid blocks is unknown. In problems where the plastic material is severely constrained by adjacent elastic material (as in the expansion of a thick-walled tube, or in the bending of a beam), the geometry of the plastic zone cannot be found.

(2) Theoretically, pressure-dependent materials must dilate during plastic deformation as a result of the associativity of plastic flow with an angle of dilatation equal to the friction angle $\psi = \phi$. However, in materials like rocks and soils, the dilatation angle is much smaller and even goes to zero after several per cent of strain. Thus, the predicted velocity field is not realistic.

Elasto-plastic non-associated plasticity

It is well known that the limiting stress for rocks and soils is approximately linearly dependent on pressure (Fig. 5a), while the flow in failure zones is close to incompressible. This behaviour cannot be described by the theory of associated plasticity where the vector of plastic deformations is orthogonal to the yield surface (Fig. 4a). Therefore, a theory of plasticity, with plastic flow independent from the failure envelope, was developed (Mandel, 1966) and called non-associated theory of plasticity.

The construction of the slip-line field for a non-associated plastic material raises a difficulty: velocity slip-lines (i.e. lines of maximum shear strain-rate) should be oriented at an angle of 45° to the direction of principal stresses, while the stress characteristics should be at an angle of $\pm(45° - \phi/2)$. The stress and strain-rate characteristics do not coincide: the direction in which material fails is not the same as that in which material can flow. Therefore, this material cannot be treated by the theory of isotropic rigid-plasticity (Vardoulakis and Salem, 1995), and elastic deformations need to be taken into account. Another consequence of non-associated plasticity is that the material deforms in a localized manner, along plastic shear zones surrounded by elastic material.

The basic assumption of elasto-plasticity is that the total strain-rate, $\dot{\varepsilon}$, is the sum of elastic $\dot{\varepsilon}^e$ and plastic strain rates $\dot{\varepsilon}^p$:

$$\dot{\varepsilon} = \dot{\varepsilon}^e + \dot{\varepsilon}^p. \tag{13}$$

Hooke's law is used for the elastic strain rate, giving

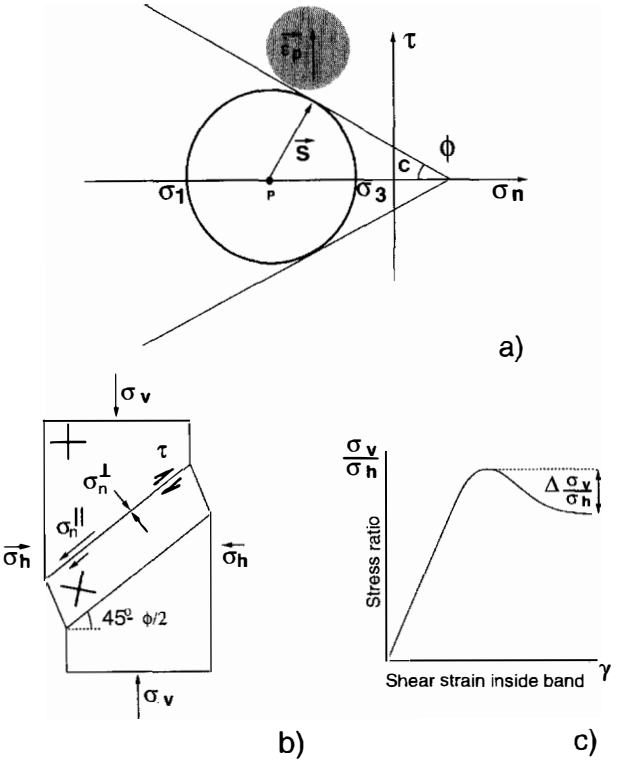

Fig. 5. (a) Yield stress for a pressure-dependent material with non-associated (incompressible) plastic flow $\phi = 0°$, $\psi = 30°$. (b) Shear band localization in a biaxial test (after Vermeer (1990)). The normal stress parallel to the band can be discontinuous. Crosses represent orientations of principal stresses. (c) 'Non-associated' softening due to decrease of mean stress inside the shear band.

$$\dot{\sigma} = D\dot{\varepsilon}^e = D(\dot{\varepsilon} - \dot{\varepsilon}^p), \tag{14}$$

where D is the elasticity matrix, $\dot{\sigma}$ and $\dot{\varepsilon}$ are stress and strain rate vectors. In the plane strain conditions and a rectangular Cartesian system, the elasticity matrix is

$$D = \begin{bmatrix} \lambda + 2G & \lambda & 0 \\ \lambda & \lambda + 2G & 0 \\ 0 & 0 & 2G \end{bmatrix},$$

where λ and G are Lamé parameters, and the vectors of stress and strain rate are

$$\sigma = (\sigma_{xx}, \sigma_{yy}, \sigma_{xy})^T \; \dot{\varepsilon} = (\dot{\varepsilon}_{xx}, \dot{\varepsilon}_{yy}, \dot{\varepsilon}_{xy})^T,$$

where the superscript T denotes a transpose.

In the literature on plasticity, a yield function f is commonly employed to distinguish plastic from elastic states. For Mohr–Coulomb materials, it can be defined as follows (Vermeer and de Borst, 1984):

$$f = \tau - p \cdot \sin(\phi) - C \cdot \cos(\phi), \tag{15}$$

where ϕ and C are the friction angle and the cohesion respectively, and τ and p are the maximum shear stress defined by equation (2) and pressure. Thus, material is in an elastic state if $f < 0$ and in a plastic state when $f = 0$ and $\dot{f} = 0$.

In the theory of plasticity, there is no direct relation

between the plastic strain and stresses because plastic deformations are irreversible and depend on the loading history. Instead, a plastic potential function g is introduced, and the plastic strain rate $\dot{\varepsilon}^p$ is assumed to be at $f=0$ as follows:

$$\dot{\varepsilon}^p = \Lambda \frac{\partial g}{\partial \sigma}, \tag{16}$$

where Λ is a scalar multiplier with no physical meaning. One of the suitable definitions of g is

$$g = \tau - p \cdot \sin(\psi) + \text{const}, \tag{17}$$

where ψ is called the dilatation angle. This angle can be measured experimentally through the increase in volume of sheared rocks. Dilatancy is due to tensile cracking and lifting of sliding blocks over asperities. However, this angle is relatively small (around 10°), and dilatation goes to zero after a few per cent of plastic strain, because rocks cannot increase in volume indefinitely. Therefore, we assume that $\psi=0$, i.e. that our material is plastically incompressible and thus conserves volume.

In order to express the constitutive model in a matrix equation, we substitute equation (16) into equation (14) to obtain:

$$\dot{\sigma} = D\dot{\varepsilon} - D\Lambda \frac{\partial g}{\partial \sigma}. \tag{18}$$

When material is in a plastic state ($f=0$), the multiplier Λ can be calculated from the condition that an element remains in a plastic state when it yields. This is the consistency condition, which can be written in matrix notation

$$\dot{f} = \frac{\partial f^T}{\partial \sigma} \dot{\sigma} = 0. \tag{19}$$

The substitution of equation (18) in the consistency condition gives

$$\dot{f} = \frac{\partial f^T}{\partial \sigma} D\dot{\varepsilon} - \Lambda \frac{\partial f^T}{\partial \sigma} D \frac{\partial g}{\partial \sigma} = 0, \tag{20}$$

from which Λ can be found. The stress–strain law can then be obtained by substituting Λ in equation (18) as is done in Vermeer and de Borst (1984):

$$\dot{\sigma} = \left(D - \frac{(D\frac{\partial g}{\partial \sigma}) \cdot (\frac{\partial f^T}{\partial \sigma} D)}{d} \right) \dot{\varepsilon}, \tag{21}$$

where

$$d = \frac{\partial f^T}{\partial \sigma} D \frac{\partial g}{\partial \sigma}.$$

Vermeer (1990) analysed the behaviour of non-associated plastic material subject to biaxial loading (Fig. 5b), where horizontal stress σ_h is kept constant but vertical stress σ_v is allowed to change. The main consequence of non-associativity is that in the post-peak regime, the material does not deform homogeneously, but bifurcates into two states: one where shear bands deform plastically and another where material outside of the band unloads elastically. This is only possible if the state of stress inside the band is different from that outside the band. The shear stress τ and normal stress perpendicular to the band σ_n are continuous across the shear band,

$$\Delta\sigma_n = 0 \Delta\tau = 0$$

as is required by the conditions of equilibrium, while the normal stress along the shear band $\sigma_n^{\parallel}$ can be discontinuous,

$$\Delta\sigma_n^{\parallel} \neq 0$$

where symbol Δ denotes the difference of stresses outside and inside of the band.

Vermeer (1990) showed that the principal stresses inside the band rotate from an angle of $(45^\circ - \phi/2)$ to 45° to the maximum compressive stress in materials with incompressible plastic flow (i.e. $\psi=0$). Thus, coaxiality between plastic strain rate and stress inside the band is satisfied. This also means that the direction of maximum plastic shear strain rate coincides with the direction of the band, while the band itself coincides with direction of failure in the stress field outside of the band (Fig. 5b).

Normal stresses parallel to the shear band $\sigma_n^{\parallel}$ decrease in the post-peak regime, which causes a decrease of vertical stress σ_v (Fig. 5c) and is

$$(\sigma_v^{\text{peak}} - \sigma_v^{\text{residual}})/\sigma_n = \frac{1+\sin(\phi)}{1-\sin(\phi)} - \frac{1+\sin(\phi)+\cos(\phi)-\cos^2(\phi)}{1-\sin(\phi)+\cos(\phi)-\cos^2(\phi)}$$

for a shear band oriented at the angle of $(45^\circ - \phi/2)$ to σ_v and a material with $\psi=0$. The decrease of stresses due to non-associativity of plastic flow is called 'non-associated softening' (Vermeer, 1990), and it is different from material softening in which the Mohr–Coulomb strength parameters, ϕ and C, are reduced as a function of plastic strain, due to damage of the material inside the fault.

Pros and cons of non-associated plasticity. This is the most complete theory of plasticity, which takes into account the Mohr–Coulomb yield criterion, the incompressible flow rule and the stress state in elastic zones. The theory predicts 'non-associated' softening and localization of deformations in pressure-dependent materials that are well observed in experiments (Vardoulakis, 1980; Vardoulakis and Graf, 1985). The same effect appears for developed faults and gouge zones in nature (Mandl, 1988; Lockner and Byerlee, 1993).

This type of rheology can be used for numerical modeling of faulting. In this approach, it is not required to prescribe the geometry and location of faults. They naturally appear where stress is concentrated, or at local heterogeneities (Hobbs and Ord, 1989; Leroy and Ortiz, 1989, 1990; Cundall, 1990; Poliakov and Herrmann, 1994).

The difficulties are mostly technical with this type of plasticity.

(1) It is not evident to use the slip-lines method, because characteristics of velocity and stresses do not coincide.

(2) Analytical solutions are not practically available.

(3) The thickness of the localization zone is not defined by the physics of the model, and the theoretical thickness of the shear band is zero. During numerical experiments, it is limited by the size of the elements of the computational grid. This means that some of the aspects of the problem can be mesh-dependent. However, the geometry and qualitative behaviour of numerically modeled shear zones should not depend on mesh resolution (Pietruszak and Mróz, 1981; Bazant *et al.*, 1984; Needleman, 1988; Sluys and de Borst, 1991).

Numerical experiments on the problem of indentation

In order to verify the predictions made in the preceding sections, we simulate the problem of indentation in the half-space numerically employing all types of plasticity considered above. We have used an explicit Lagrangian technique similar to FLAC, as developed by Cundall and Board (1988) and Cundall (1989), to simulate an elasto-plastic two-dimensional medium under the plane-strain condition. FLAC is a very powerful technique for simulating non-linear rheological behaviour at high resolution mesh because it uses an explicit time-marching scheme that does not require storage of large matrices, which are typical of implicit methods.

Figure 6(a–d) summarizes our numerical experiments of the indentation problem for the three types of plasticity discussed above. Only a half of the domain is simulated. The die is represented by the application of vertical velocities at the left upper corner of the domain. Figure 6(a) shows the typical initial stage of deformation, which is similar for all rheological models. The left part of Fig. 6(a) shows the plastic (i.e. failure) zone in white and the elastic zone in black, and the right part shows the velocity and strain rate fields. The geometry of the plastic zone is similar to the one predicted by the 'elastic' solution (Fig. 2a) and not by any of the plastic solutions (Fig. 2b–d). It would difficult to anticipate such a result beforehand, whereas it can be readily explained by looking at numerical results. One can see that in the initial stages of the penetration of the die, the plastic zone is severely constrained by the elastic material outside, and the geometry of the plastic zone is controlled by the distribution of elastic stresses outside of this zone. Thus, in the theory of rigid-plasticity, neglecting the distribution of stresses outside of plastic zone fails to predict this result. On the contrary, the 'elastic' solution gives a qualitatively correct prediction (Fig. 2a) because the stresses in the failure zone are not far from the yield stresses for small deformations.

However, the situation becomes different as deformations increase. Figure 6(b & c) shows numerical solutions for associated pressure-independent ($\phi = 0°$) and pressure-dependent ($\phi = 30°$) plasticities, respectively, which are very similar to the analytical rigid-plastic solutions (Fig. 2b–d). One can also see that our numerical solution is closer to the Prantdl type than to Hill type, probably because our boundary conditions are kinematic and not in stresses. The case of non-associated plasticity (Fig. 6d) is the most interesting because it was difficult to predict theoretically. One can see that this solution is a mixture between the previous two: while slip-lines under the die resemble the case with $\phi = 30°$, they come out at the surface as in the case with $\phi = 0$. This is not a coincidence. The zones of localization in non-associated plasticity should form in between the velocity and stress slip-lines, which are solutions for associated plasticity when $\phi = 0°$ and $\phi = 30°$, respectively. We also found an agreement between the calculated and predicted critical loads (equations (9) and (12)), while the non-associated plasticity case gave a result close to equation (12). The last solution can be explained by comparing the 'complete' solution of Bishop (1953) and the plot of elastic and plastic zones in Fig. 6(e). 'Complete' solutions consist of all possible solutions for stress slip-lines without consideration of the kinematics of plastic flow (Fig. 6, left). Our result (Fig. 6, right) shows that plastic zones are similar to some parts of the 'complete' solution. However, the deformations in deep failure zones under the die are very small because they are hindered by the surrounding elastic material. The majority of deformations are accommodated along curved shear zones connected to the free-surface because the slip along these zones is not affected by the surrounding media.

These results demonstrate that 'elastic' solutions predict the geometry of failure zones fairly well when plastic deformations are comparable to the elastic ones, and/or when a failure zone is constrained by the elastic material outside the zone. The theory of rigid-plasticity correctly predicts the geometry of the failure zones for large deformations, when a plastic zone is connected to a free surface. Non-associated elasto-plasticity gives the most complete solutions, with failure zones evolving with time. However, the combination of 'elastic' and 'rigid-plastic' approaches can qualitatively predict the right mode of failure.

COMPRESSION WITH A BASAL SHEAR

The geometry and evolution of faults in thrust sheets and accretionary prisms are not yet completely understood. This problem is related to 'the paradox of large overthrusts' (Price, 1988): how is it possible to displace a long and thin thrust sheet as a coherent unit over a frictional surface by pushing it from behind? The maximum length of the thrust sheet along which it is possible to move is limited by the strength of the rock. A simple estimation of this length for a rectangular block

a) Initial stage

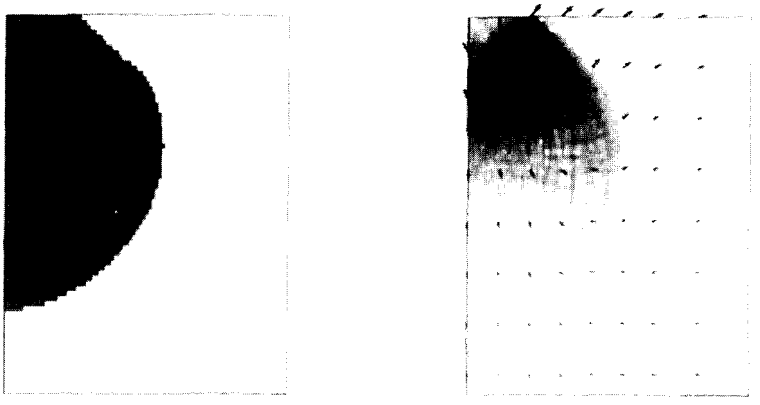

Advanced stage

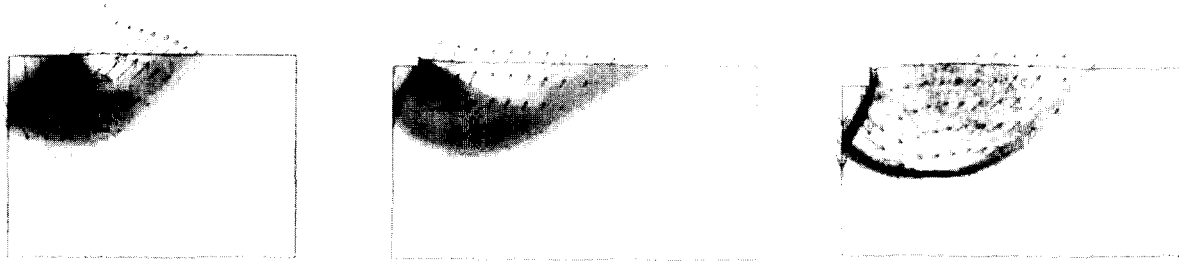

b) $\phi = 0, \psi = 0$ c) $\phi = 30, \psi = 30$ d) $\phi = 30, \psi = 0$

e) Complete solution

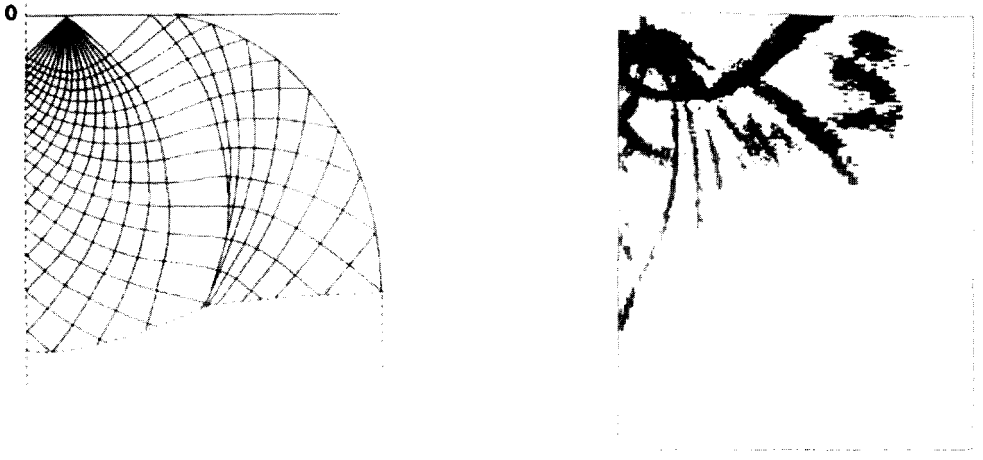

Fig. 6. Numerical verification of analytical predictions of indentation in an elasto-plastic material. Only right-half of the problem is shown due to symmetry. The top surface is stress-free, and a vertical velocity is applied on the top. Bottom and right boundaries are free-slip. We have chosen Poisson's ratio $\upsilon = 0.25$, Lamé's parameters $\lambda = G = 3.10^{10}$ Pa for all numerical experiments in the paper. (a) Initial stage of indentation is independent of friction angle and dilatancy. Left figures show that geometry of plastic zone (grey) embedded in elastic material (white) is in agreement with the 'elastic' prediction in Fig. 2(a), Velocity field and strain rate fields are shown on the right. (a) and (b) large deformations solutions for associated ($\phi = \psi = 0$) (b) and ($\phi = \psi = 30°$) (c) plastic materials are in agreement with Prantdl's solutions (Fig. 2b & d). (d) Solution for a material with 'non-associated' flow rule ($\phi = 30°$, $\psi = 0$) is a mixture of the two previous solutions with associated flow rule. (e) Left: the complete analytical solution proposed by Bishop (1953) for associated plasticity with $\phi = 0$. Right: a snapshot of numerically obtained plastic zones (grey) for non-associated plasticity ($\phi = 30°$ and $\psi = 0$).

pushed from the rear gives values that are orders of magnitude below those observed in nature (Hubbert and Rubey, 1959; Jaeger and Cook, 1969). Currently, there are two non-mutually exclusive explanations: (a) pore fluid pressure at the base of a thrust effectively decreases the friction force (Hubbert and Rubey, 1959); and (b) a thrust with a wedge geometry can be at yield stress in all its parts and thus move as one unit (Chapple, 1978). The extension of his theory for a pressure-dependent plastic material was worked out by Davis *et al.* (1983) and Dahlen (1990). Here, we proceed in the same way as in the previous section, showing elastic, rigid-plastic and elasto-plastic solutions for both rectangular and wedge geometries of a thrust sheet.

Elastic solutions

Rectangular geometry. Hafner (1951) was probably the first to apply the theory of Anderson for calculation of fault pattern in a thrust zone. Consider a rectangular block of horizontal dimension L (Fig. 7a) in a gravity field. The pushing force applied at the left boundary of the block is in equilibrium with the shear stress at the bottom. Assuming that shear stress σ_{xy} linearly changes with depth, one can find a simple stress field satisfying the equations of equilibrium,

$$\begin{aligned} \sigma_{xx} &= \rho g y + c(x - L) \\ \sigma_{yy} &= \rho g y \\ \sigma_{xy} &= -cy. \end{aligned} \tag{22}$$

For different values of c, one can find the part of the domain where shear stress exceeds the yield stress (equation (1)) and predict the direction of failure zones as lines oriented at $\pm(45° - \phi/2)$ to the direction of maximum compressive stress (Fig. 7a).

Wedge geometry. A typical example of an application of an 'elastic' solution for fault prediction for accretionary prisms is shown in Fig. 7(b) (after Yin

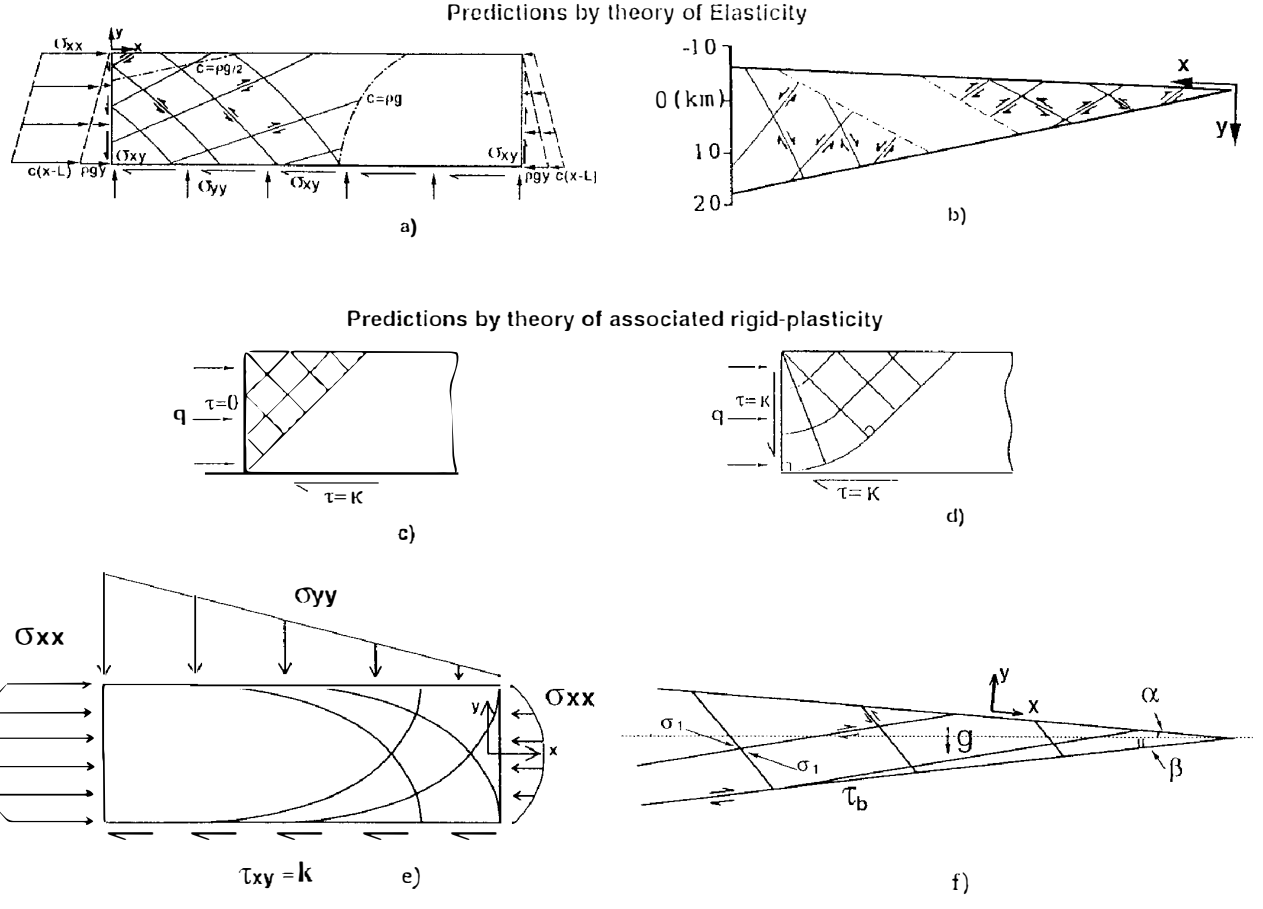

Fig. 7. Analytical solutions for faulting in a thrust zone. (a) Trajectories of potential faults (solid lines) from Hafner's solution (Hafner, 1951) for compression of an elastic rectangular block with a basal shear. Dashed lines bound predicted zones of failure for different values of the basal shear ($c = 0.2\,\rho gH$ and ρgH). (b) Yin's solution (Yin, 1993) for a particular stress distribution in compressed elastic wedge. (c) Slip-lines in a block pushed above a base of strength k. The left boundary is shear-stress-free. (d) The same as (c) with the shear stress, k, applied at the left boundary. Note curved 'listric' slip-lines in this case compared to the straight slip-lines in (c). (e) Solution of Prantdl (after Hill (1950)) for the compression of a rigid-plastic block with strength k between two rough plates with cohesion k. Note curved slip-lines (cycloids), and an increase of vertical stress from right to left. (f) Fault trajectories in a cohesionless rigid-plastic wedge ($\phi = \psi = 30°$, $C = 0$) pushed over a frictional base (after Dahlen (1984)).

(1993)). Here, the author assumed the following distribution of stresses in the wedge,

$$\begin{aligned}\sigma_{xx} &= k_3 x + k_4 y + k_8 + \rho g x \cdot \sin \alpha \\ \sigma_{yy} &= -\rho g y \cdot \cos \alpha \\ \sigma_{xy} &= -k_3 y.\end{aligned} \tag{23}$$

The three parameters k_i were freely varied to obtain 'paradoxical' fault geometries. There are thrust faults at the toe of the wedge and normal faults in the rear of wedge. This is the result of an arbitrarily chosen elastic stress field, due to unjustified stress boundary conditions. For example, in the case shown in Fig. 7(b), basal friction is greater than the internal friction in the wedge, shear stress changes sign along the bottom depending on the length of the wedge, and terms k_8 and k_4 ambiguously describe compressive stress coexisting with extensive stress. While Yin assumed a Mohr–Coulomb criterion for directions of failure zones, he delimited the unstable zones by a maximum shear stress cut-off of 50 MPa, independent of the pressure. Several examples of other inappropriate applications of 'elastic' solutions to the problem of faulting are discussed by Buck (1989) and Wills and Buck (1997).

Plastic solutions

Rectangular geometry. Let us apply the slip-line theory for the problem of the sliding of a plastic rectangular block on a base with cohesive strength k and friction angle $\phi = 0$ (Fig. 7c & d). If there is no shear stress applied to the left boundary and only a normal horizontal stress, the slip-lines are at 45° to the boundary and form a triangle (Fig. 7c). If the shear stress, k, is applied to the left boundary, then the boundary becomes a slip-line itself, changing the slip-line field to the configuration shown in Fig. 7(d). It is interesting to note the application of shear stress at the curving left boundary faults, compared to the shear-stress-free boundary condition that gives straight faults. This simple example shows that it is impossible to move the rectangular block as a unit by a simple push from the rear.

Let us find a condition when the entire block will be at yield stress and thus flows plastically. One of the possibilities is a compression of a block between two rough plates (Fig. 7e). The horizontal dimension of the problem is assumed to be larger than the height H. The solution for the pressure-independent material with cohesion k was given by Prantdl. The stress distribution is

$$\begin{aligned}\sigma_{xx} &= cx \pm 2\sqrt{k^2 - y^2 \cdot c^2} \\ \sigma_{yy} &= cx \\ \sigma_{xy} &= -cy,\end{aligned}$$

where $c = k/H$ (Hill, 1950). Stresses at the boundary of the domain are shown in Fig. 7(e) as well as slip-lines, which are cycloids. The bottom half of the problem may represent a thrust pushed from the left which slides at the lower surface with basal friction k. One can see that the necessary condition to render the whole block plastic is the linear load at the surface, which may be represented by topographic slope. It is interesting to notice that the cycloids may represent curved 'listric' faults. Examining Fig. 7(d & e), one can conclude that faults are curved if the bottom boundary is a slip line. This also means that the friction angle of the base should be equal to that of the wedge.

Wedge geometry. Following the idea of Chapple (1978), Davis *et al.* (1983) considered a thrust with a geometry of a wedge (Fig. 7f), which is at the verge of plastic failure. Dahlen (1984) found an analytical solution for the equilibrium of a cohesionless Coulomb wedge, which is bounded by a plane of weakness from below. It was assumed that the stresses σ_{yy} and σ_{xy} acting at the plane parallel to x are caused only by the gravity force (Terzaghi, 1943),

$$\sigma_{yy} = \rho g y \cos(\alpha) \qquad \sigma_{xy} = -\rho g y \sin(\alpha), \tag{24}$$

where g is the acceleration of gravity and ρ is the density of the wedge. It is easy to see that these stresses satisfy equilibrium conditions

$$\begin{aligned}\frac{\partial \sigma_{xx}}{\partial x} + \frac{\partial \tau_{xy}}{\partial y} + \rho g \sin(\alpha) &= 0 \\ \frac{\partial \sigma_{yy}}{\partial y} + \frac{\partial \tau_{xy}}{\partial x} - \rho g \cos(\alpha) &= 0,\end{aligned} \tag{25}$$

and the following conditions are fulfilled

$$\frac{\partial \sigma_{xx}}{\partial x} = \frac{\partial \tau_{xy}}{\partial x} = 0. \tag{26}$$

This means that the stress does not change at the line parallel to axis x, and the orientations of principal stresses are the same everywhere in the wedge. Thus, a non-cohesive critical wedge is self-similar in the sense that a magnified version of any portion of it near the toe is indistinguishable from the wedge as whole. This is a consequence of the absence of an inherent length scale in the equations of equilibrium and in the boundary and failure conditions (Dahlen, 1990). Slip-lines also have the same directions everywhere in the wedge, being oriented at $\pm(45° - \phi/2)$ angles to σ_1 (Fig. 7f).

Dahlen (1990) gives an approximate solution for the equilibrium of a wedge with a narrow taper ($\alpha \ll 1$, $\beta \ll 1$), which is appropriate for most of the thrusts in nature. If the coefficient of friction at the base is μ_b and the coefficient of pore pressure in the wedge and at the base are λ and λ_b, respectively, then

$$\alpha + \beta \approx \frac{\beta + \mu_b(1 - \lambda_b)}{1 + 2(1 - \lambda)\sin(\phi)/(1 - \sin\phi)}. \tag{27}$$

This equation shows that the critical taper $(\alpha + \beta)$ is increased by an increase in the coefficient of basal friction μ_b or an increase in the coefficient of pore pressure λ, whereas it is decreased by an increase in the internal

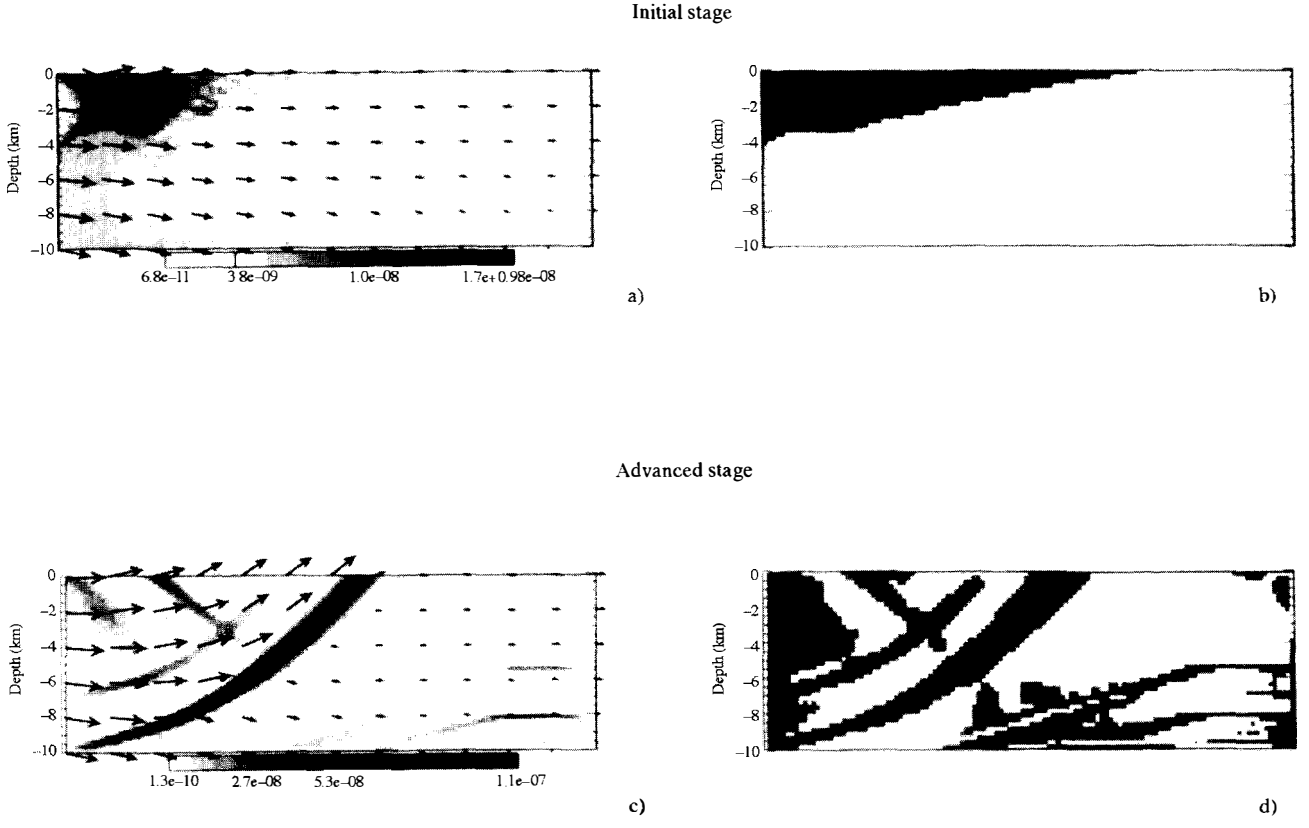

Fig. 8. Numerical modelling of Hafner's problem (Hafner, 1951) for elasto-plastic material ($\phi = 30°$, $\psi = 0°$ and $C = 20$ MPa). The simulated region is 10 km high and 30 km long. Kinematical boundary conditions are given by equation (22). Left figures show velocity field and strain rate at initial (a) and advanced (c) stages. Plastic (grey) zones (b) and (d) are shown on the right and resemble elastic (Fig. 7a) and rigid-plastic (Fig. 7d) analytical predictions.

friction angle ϕ or increase in the coefficient of pore pressure at the base λ_b.

Numerical solutions

Rectangular geometry. It is not always simple to compare elastic and plastic solutions for the same problem due to differences in application of boundary conditions. Elastic solutions considered here are formulated with stress boundary conditions, whereas, it is difficult to apply the same stresses for a plastic material. These stresses may be above the yield stress, making the problem ill posed. It is more practical to apply velocity boundary conditions for plastic problems, so that material is gradually loaded by deforming boundaries allowing a gradual growth of plastic zones. Therefore, in order to compare the 'elastic' solution of Hafner with an elasto-plastic solution, we expressed the stresses from equation (22) in terms of velocities. If one assumes that shear stress σ_{xy} grows linearly with time, then it should be compensated by an increase of normal stress σ_{xx} as follows from the equation of equilibrium,

$$\sigma_{xy}(t) = c \cdot y \cdot t \qquad \sigma_{xx}(t) = -c \cdot x \cdot t,$$

where c is the rate of the stress increase chosen from consideration of numerical stability and t is time. One can integrate these equations to obtain the velocity field V_x, V_z corresponding to this loading:

$$V_x = A \cdot c \cdot \left(\frac{x^2}{2} - L \cdot x\right) + \left(B - \frac{1}{G}\right) \cdot c \cdot \frac{y^2}{2} \qquad (28)$$
$$V_y = -B \cdot c \cdot (x - L) \cdot y$$

$$A = \frac{\lambda + 2G}{4G(\lambda + G)} \qquad B = \frac{\lambda}{4G(\lambda + G)},$$

where λ and G are the Lamé parameters, and L and H are the horizontal and vertical dimensions of the problem. These velocities were applied at the boundaries as shown in Fig. 8(a & c). Plastic zones are shown in white in Fig. 8(b & d). At the initial stages (Fig. 8a & b) when deformations are small, the 'elastic' solution of Hafner (Fig. 7a) predicts well the geometry of the plastic zone as in the example of indentation. However, when the whole region becomes plastic (bottom of Fig. 8c & d), the rigid-plastic slip-lines (Fig. 7d) predict faulting better, especially the geometry of curved shear bands, which is due to a strong basal shear (Mäkel and Walters, 1993).

Wedge geometry. We also have verified numerically the prediction of the rigid-plastic model of Dahlen (1984) for the cohesionless wedge. Boundary conditions are shown

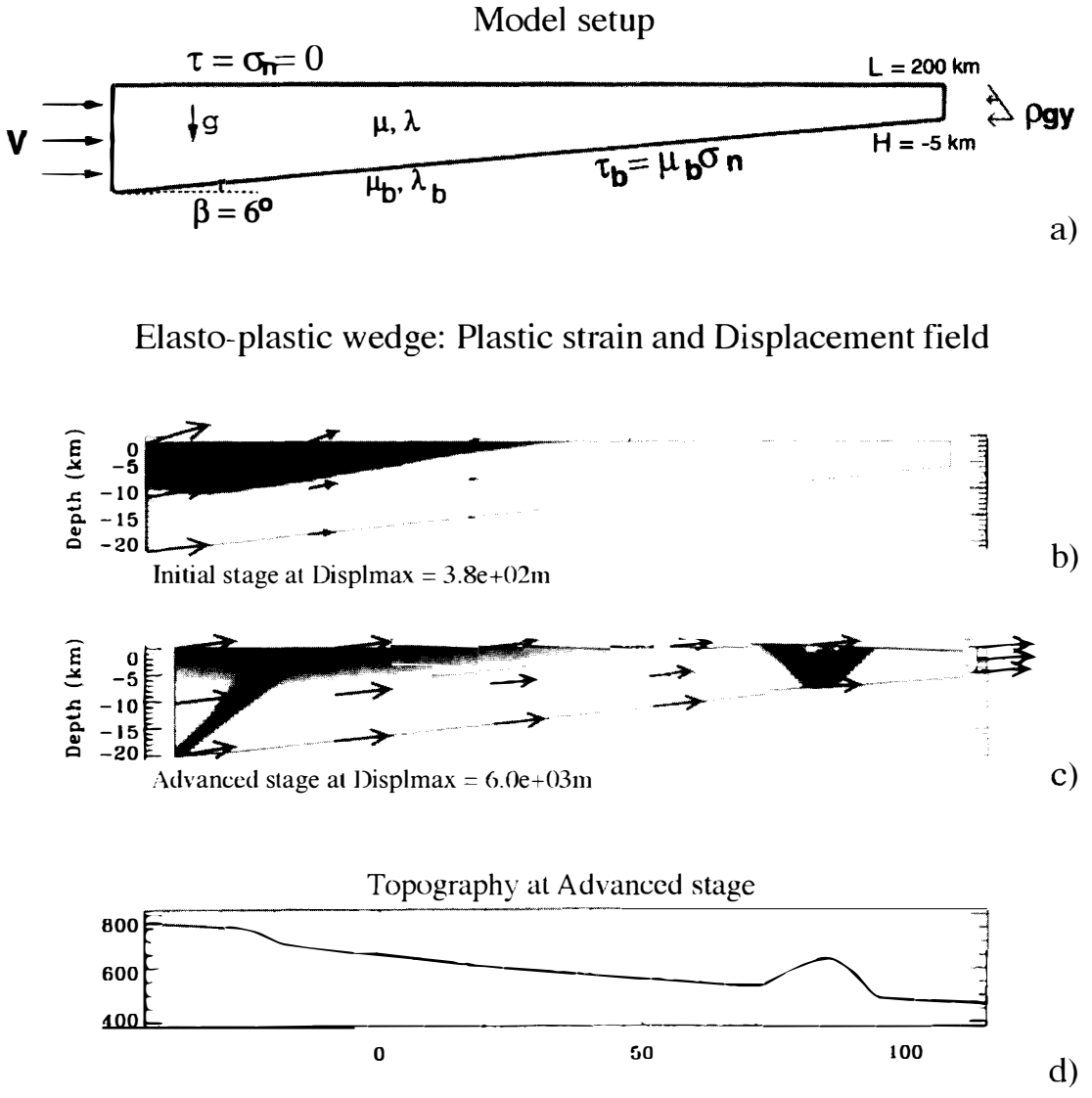

Fig. 9. Numerical modelling of faulting in a frictional cohesionless wedge. (a) Numerical setup. Constant horizontal velocity and zero shear stress applied on the left border and hydrostatic stresses on the right. Upper surface is initially horizontal ($\alpha = 0$) and stress-free. The base is inclined at the angle $\beta = 6°$. Friction angles in the wedge (ϕ) and at the base (ϕ_b) are 30°. Coefficients of fluid pore pressure are $\lambda = \lambda_b = 0$–4. Two snapshots corresponding to the displacement of the left border for 38 m (b) and 6 km (c) demonstrate the development of the failure zone from the upper surface to the base. The slope increases to the critical value and then the wedge starts to slip as a whole, simultaneously deforming internally. (d) Topography has an average critical slope of 5° and a bulge of 200 m on the right side due to a local thrust.

in Fig. 9(a). The parameters of the problem were chosen as follows: the slope of the base β is 6°, the top surface is initially flat ($\alpha = 0$), the coefficient of pore pressure $\lambda = 0.4$ for the base, and the angle of friction for the wedge $\phi = \pm(45° - \phi/2)$. Figure 9(b & c) shows the evolution of plastic zones with time. At the initial stage (Fig. 9b), only the rear part of the wedge slides and the geometry of the plastic zone are similar to that predicted by Hafner's solution for a rectangular block (Fig. 7a) for $c = 0.2\ \pi gy$. As loading continues, the zone of plastic deformations increases laterally and vertically, until the slope of the wedge builds up such that the whole block starts to slide (Fig. 9c). We found that the theoretical prediction of the wedge taper (equation (20)), which predicts a value of $\alpha = 5.75°$, is in agreement with that obtained numerically ($\alpha = 5°$) by measuring the average topographic slope in Fig. 9(d).

Although the theory of Dahlen (1984) gives a very good estimation of the average slope, it does not tell us about the evolution of faults with time. It can be seen from the numerical experiments that faults are not stable and that active faults jump from one place to another, because the stress distribution in the thrust is not uniform and changes in time. This is because slip at any fault is resisted by gravitational forces and is not kinematically compatible with slip along the base. Therefore, active faults constantly change their positions, creating a complex, evolving network of faults accommodating the bulk deformation of the thrust sheet. However, if the critical surface slope α is reached, movement of the entire

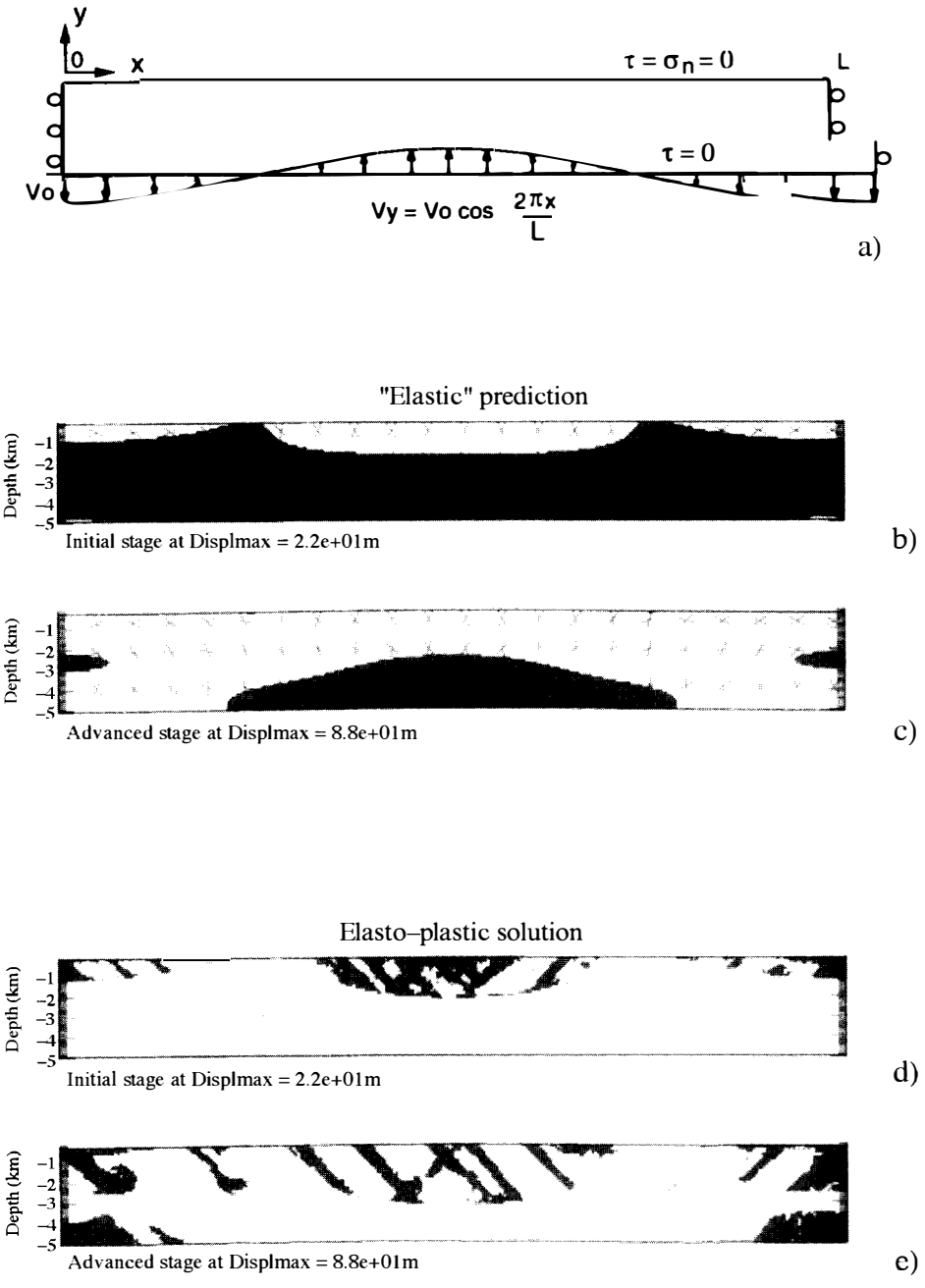

Fig. 10. Prediction of faulting due to bending. (a) Numerical setup: vertical borders are free-slip, and upper surface is stress-free. The bottom boundary is shear-stress-free and subjected to a sinusoidal velocity. Angle of friction ϕ is 30° and cohesion is 5 MPa. Potential zones of failure (white color) and trajectories of faults in elastic material are shown for two displacements of bottom boundary 22 m (*b*) and 88 m (*c*). Elasto-plastic solutions (d and e) for the same amounts of maximum displacements of 22 and 88 m. Plastic shear bands (in grey) terminate at the boundary with elastic domain, and thus elasto-plastic solution closely resembles the elastic one. Note that at the later stage, the top zones of failure are disconnected from the bottom ones, contrary to the elastic predictions.

thrust wedge can occur without internal deformations, while the whole wedge is at critical stress.

PLATE BENDING

Faulting in plates due to bending is an important problem in geophysics. The distribution of stresses in thick plates (i.e. with characteristic dimensions of the same order as the thickness of a plate) was studied in order to predict low-angle faulting under particular boundary conditions (Hafner, 1951; Sanford, 1959; Spencer and Chase, 1989). One can find a discussion on prediction of low-angle faulting due to flexural stresses in Wills and Buck (1997).

Here, we consider plate bending under loads with a wavelength considerably longer than the thickness of the plate (Fig. 10a). Thus, our results can be interpreted in

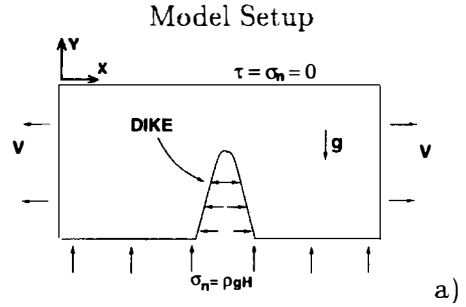

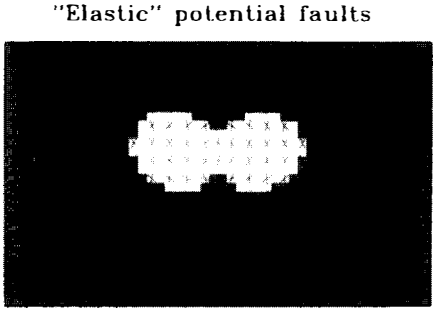

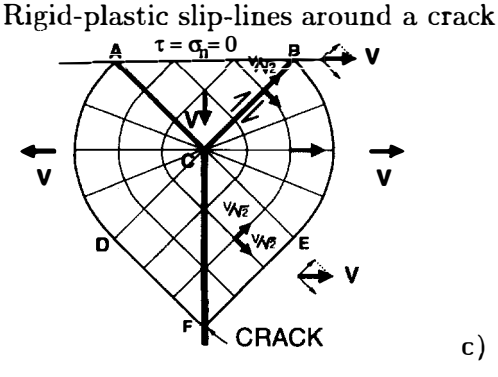

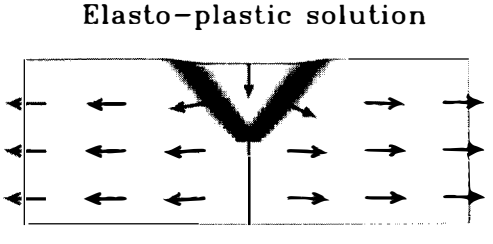

Fig. 11. Prediction of faulting around a dike. (a) Numerical setup: constant lateral velocities, stress free upper boundary, Winkler's foundation at the bottom, hydrostatic pressure in the dike and no density contrast between the solid and fluid phases. (b) Prediction of faulting by theory of elasticity. The zone of failure (in white) is embedded in elastic material around (grey). Trajectories of potential faults are sub-horizontal at the tip of the dike. (c) Slip-line pattern predicted by pressure-independent associated plasticity around a mode-I crack. A rigid triangle above the crack slides along straight slip-lines inclined at 45° to the free surface. (d) Velocity field and accumulated plastic strain obtained by numerical simulation of the problem in an elasto-plastic material. This solution is in agreement with the 'slip-line' solution.

terms of thin plate theory (Timoshenko and Woinowsky-Krieger, 1959; Turcotte and Schubert, 1982), which is fairly accurate for many geophysical applications. It can be shown that shear stresses in thin plates and at small deflections are considerably smaller than normal stresses. Thus, the directions of principal stresses are very close to horizontal and vertical, and faults will be formed at $\pm(45^\circ + \phi/2)$ to the surface in zones of extension and at $\pm(45^\circ - \phi/2)$ in zones of compression. The geometry of failed zones then depends on the geometry of loading and is controlled by the stresses in elastic parts of the plate. Thus, bending of a thin plate is an example where an 'elastic' solution may provide a good guide for geometry of faulting. However, the theory of rigid-plasticity cannot predict the geometry of plastic zones, because stresses outside the plastic zones are not calculated. Therefore, here we compare only 'elastic' and 'elasto-plastic' numerical solutions, without considering the 'rigid-plastic' case.

We apply a sinusoidal vertical velocity at the bottom with zero shear stress (Fig. 10a):

$$V_y(y = H) = V_o \cos\left(\frac{2\pi x}{L}\right) \qquad \tau(y = H) = 0,$$

free slip at lateral boundaries and free-stress boundary conditions at the surface. Figure 10(b & c) demonstrates white zones where elastic stresses exceed the yield condition and thus potential zones of failure for two vertical displacements V_o. The results of bending of an elasto-plastic plate are shown in Fig. 10(d & e). One can see that the 'elastic' solution predicts very well the zones of failure and the directions of failure for deflections in the order of 50 m, and less successfully for larger displacements. The slip along individual faults cannot be large, because faults terminate at the boundary with intact material; therefore, active faults change their position as in the example of the thrust wedge. In this way, the slip on numerous closely spaced discrete faults accommodates bending.

This example shows us again that for small deformations, and when the failure zones are tightly constrained by elastic material, 'elastic' solutions (Fig. 10b & c) predict fairly well the intergrated effect of slip on individual faults. At larger strains, a single fault may cut through the entire plate. The transition from bending on distributed faults to breakage by a single fault is studied by Buck (1997).

FAULTING AROUND A DIKE

Parsons and Thompson (1993) proposed an idea to explain the low-angle faulting in the Basin and Range Province as a result of extension in a zone of active magmatism. They suggested that the stress distribution in the elastic media around a dike (adopted from Pollard and Segall, 1987) favours low-angle faulting. We repro-

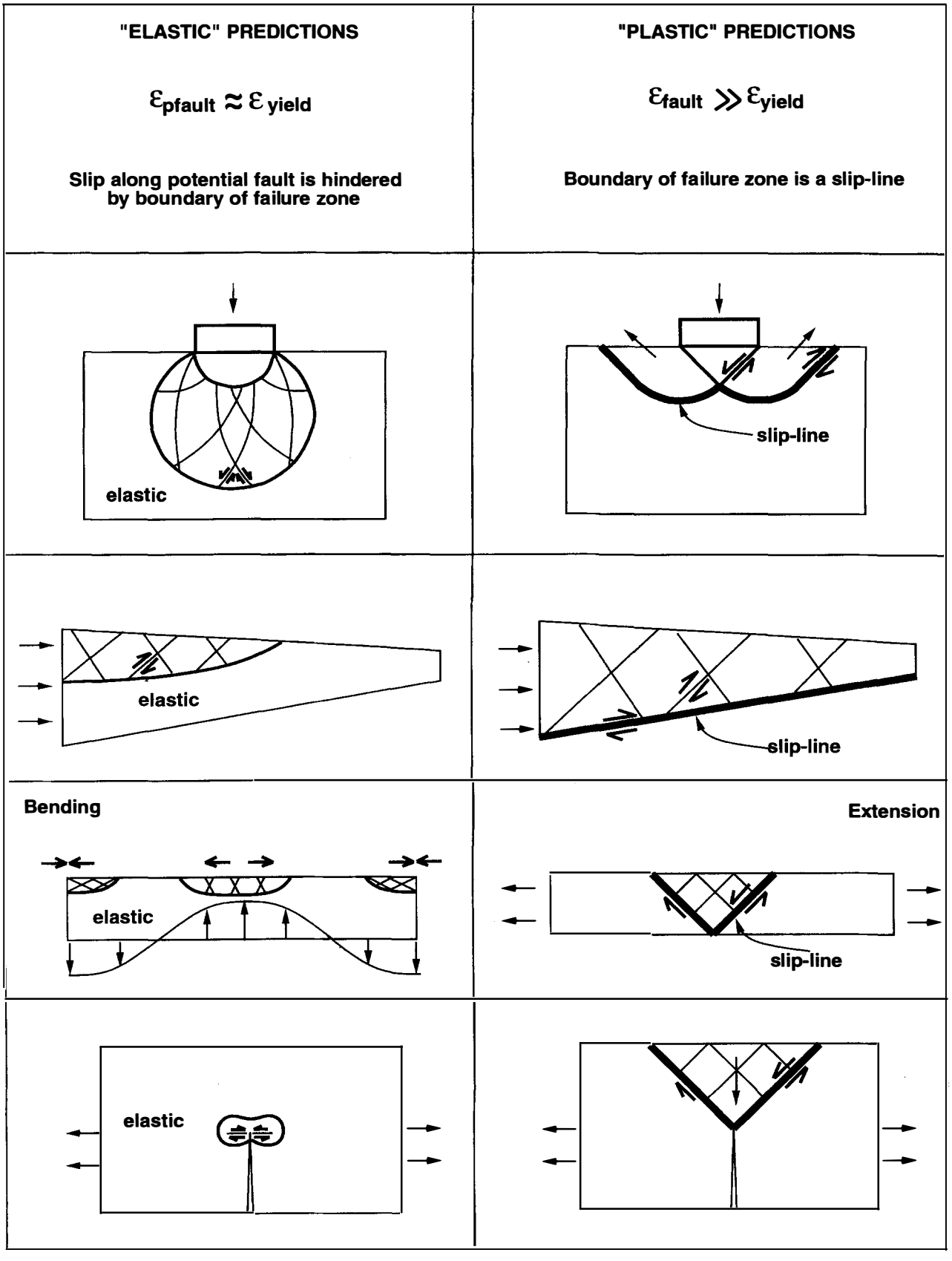

Fig. 12. Fault patterns for small (left column) and large (right column) deformations for the problems considered in the paper (from the top to the bottom): indentation of a die into a half-space, thrusting with basal shear, extension due to bending (left) and stretching (right), influence of a dike on normal faulting. Elastic solutions predict faulting correctly for zones of failure constrained by surrounding elastic material. Rigid-plastic solutions give correct predictions when failure zones are bounded by a slip-line that is connected to the free-surface or a zone of weakness.

duce an 'elastic' solution with the following boundary conditions: a stress free upper boundary, hydrostatic pressure at the bottom (Winkler's foundation), constant velocities applied at the lateral boundaries and hydrostatic fluid pressure in the dike (Fig. 11a). There is no variation of densities between solid rock, magma and inviscid substratum.

Directions of potential faults predicted by elasticity are shown in Fig. 11(b). One can see that low-angle faults may appear in small zones around the tip of the dike. They terminate in the surrounding elastic media and cannot accommodate large displacements. This point is also discussed by Wills and Buck (1997).

We have also constructed a slip-line field around a mode-I crack in a pressure-independent rigid-plastic material (Fig. 11c). This solution cannot be directly compared to the studied case, because it does not take into account the gravity forces and dependence of the yield stress on pressure, but it gives an idea of how faults can be formed. We modified the classical solution for a mode-I crack (e.g. Kachanov, 1974; Unger, 1995) to take into account the upper free-surface. First, we constructed three triangles ABC, FDC, FEC that are adjacent to shear stress free boundaries: the upper surface and a crack. Thus, slip-lines are straight in these domains, and they move as rigid blocks. Two zones, ACD and BCE, make the rest of the slip-line field. It can be seen that this problem is similar to Prantdl's die solution; therefore, the limiting stress in the zone ACB is also given by the equation $\sigma_{xx}=k(\pi+2)$ (Unger, 1995), where k is the maximum shear stress. The velocity field can be constructed following the rules that the normal component of velocity is continuous across slip-lines and should equal the velocity of a rigid block, while the tangential component may be discontinuous. We constructed the following velocity field: the block ABC moves downwards as one unit with constant velocity V and two domains ADFC and BEFC moves as one unit laterally with the same velocity. Velocities are discontinuous across the lines AC and BC which can be potential faults. The jump in tangential velocities equals $2\sqrt{2}V$.

We also modelled numerically the problem shown in Fig. 11(b) using a Mohr–Coulomb elasto-plastic material. Figure 11(d) clearly shows two normal faults connecting the tip of the dike with the free surface as predicted by rigid-plastic theory. The slip along these faults eliminates the possibility of low-angle faulting. This example shows that prediction of faulting by 'elastic' solutions may be erroneous if the kinematics of potential faults is not taken into account.

CONCLUSIONS

In this paper, we applied several simple approaches for fault prediction to some idealized geological problems. Comparison of these results reveals the strength and limits of each method, and these are compiled and summarized in Fig. 12, to draw general conclusions. The left column of Fig. 12 shows a sketch of the faulting predicted from 'elastic' solutions. The right column shows the same problems resolved by using the theory of plasticity (except for the problem of bending, which is replaced by uniform tension).

The 'elastic' solutions (Fig. 12 left) predict zones of failure reasonably well under the following conditions:

(1) The stress field is close to the yield stress, in other words, strain on potential faults ε_{pf} is of the same order as the limiting strain ε_{yield}.
(2) Zones of failure are severely constrained by surrounding elastic material.
(3) Lines of failure are terminated at the boundary between intact and failed material.

The theory of rigid-plasticity (Fig. 12 right) is appropriate for the following reasons:

(1) Slip along failure zones can accommodate large deformation $\varepsilon_f \gg \varepsilon_{yield}$;
(2) Zones of failure are bounded by a slip-line which allows material to deform in a failure zone which is somehow detached from the material outside;
(3) Lines of failure do not terminate in surrounding intact material, and/or they are connected to a free surface, a viscous substratum or a zone of weakness.

In contrast to the theories of elasticity and rigid-plasticity, the theory of elasto-plasticity allows modelling of the initiation of failure as well as large deformations along faults. Additionally, this method describes the complex spatio-temporal evolutions of faulting. Figures 6(e), 8(c) and 9(c) give a taste of how more realistic faults can be modelled, different from those predicted by the simpler theories.

Acknowledgements—This paper is a result of numerous discussions over a long period of time with Yuri Podladchikov, Roger Buck, Ethan Dawson, Peter Cundall, Hans Herrmann, Geoffrey King, Jean Chery, Jacques Malavieille and Serge Lallemand. Amy Clement and Ethan Dawson gave the English of this paper an inimitable American touch.

REFERENCES

Anderson, E. M. (1951) *The Dynamics of Faulting and Dike Formation*. Oliver and Boyd, Edinburgh.
Backhofen, W. A. (1972) *Deformation Processing*. Addison-Wesley, Reading, MA.
Bazant, Z. P., Belytschko, T. B. and Chang, T. B. (1984) Continuum theory for strain softening. *ASCE Journal of Engineering Mechanics Division* **110**, 1666–1692.
Bishop, J. F. W. (1953) On the complete solution to problems of deformation of a rigid plastic material. *Journal of the Mechanics and Physics of Solids* **2**, 43–53.
Buck, W. R. (1990) Comments on 'Origin of regional, rooted low-angle normal faults' by An Yin. *Tectonics* **9**, 545–546.
Buck, W. R. (1992) Effect of lithospheric thickness on the formation of high- and low-angle normal faults. *Geology* **21**, 933–936.
Buck, W. R. (1997) Bending thin lithosphere causes localized 'snapping' and not distributed 'crunching': Implications for abyssal hill formation. *Geophysics Research Letters* **24**(20), 2531–2534.
Byerlee, J. (1978) Friction of rocks. *Pure and Applied Geophysics* **116**, 615–626.

Byerlee, J. D. and Savage, J. C. (1992) Coulomb plasticity within the fault zone. *Geophysics Research Letters* **19**(23), 2341–2344.
Chapple, W. M. (1978) Mechanics of thin skinned fold-and-thrust belts. *Bulletin of the Geological Society of America* **89**, 1189–1198.
Crouch, S. L. and Starfield, A. M. (1990) *Boundary Element Methods in Solid Mechanics*. Unwin Hyman, London.
Cundall, P. and Board, B. (1988) A microcomputer program for modeling large-strain plasticity problems. In *Proceedings of the 6th International Conference on Numerical Methods in Geomechanics*. Innsbruck, Austria, pp. 2101–2108.
Cundall, P. A. (1989) Numerical experiments on localization in frictional materials. *Ingenieur Archiv.* **59**, 148–159.
Cundall, P. A. (1990) Numerical modeling of jointed and faulted rock. In *Mechanics of Jointed and Faulted Rocks*, ed. A. A. Rossmanith, pp. 11–18. Balkema, Rotterdam.
Dahlen, F. A. (1984) Noncohesive critical Coulomb wedges: an exact solution. *Journal of Geophysical Research* **89**(B12), 10125–10133.
Dahlen, F. A. (1990) Critical taper model of fold-and-thrust belts and accretionary wedges. *Annual Reviews in Earth and Planetary Science* **18**, 55–99.
Davis, D., Suppe, J. and Dahlen, F. A. (1983) Mechanics of fold-and-thrust belts and accretionary wedges. *Journal of Geophysical Research* **88**(B2), 1153–1172.
Forsyth, D. W. (1992) Finite extension and low-angle normal faulting. *Geology* **20**, 27–30.
Hafner, W. (1951) Stress distributions and faulting. *Bulletin of the Geological Society of America* **62**, 373–398.
Hassani, R. and Chéry, J. (1996) Anelasticity explains topography associated to Basin and Range normal faulting. *Geology* **23**, 1095–1098.
Hassani, R., Jongmans, D. and Chéry, J. (1996) 2D numerical modeling of oceanic subduction. *Journal of Geophysical Research*, submitted.
Hill, R. (1950) *The Mathematical Theory of Plasticity*. Oxford Sciences Publications, Ely House, London.
Hobbs, B.E., Mühlhaus, H.B. and Ord, A. (1990) Instability, softening and localization of deformation. *Geological Society Special Publication* **54**, 143–165.
Hobbs, B. E. and Ord, A. (1989) Numerical simulation of shear band formation in frictional-dilational material. *Ingenieur Archives* **59**, 209–220.
Hubbert, M. K. and Rubey, W. W. (1959) Role of fluid pressure in mechanics of overthrust faulting: (1) Mechanics of fluid-filled solids and its application to overthrust faulting. *Bulletin of the Geological Society of America* **70**, 115–166.
Jaeger, J. C. and Cook, N. G. W. (1969) *Fundamentals of Rock Mechanics*. Methuen and Co., London.
Johnson, J. and Mellor, P. B. (1983) *Engineering Plasticity*. Ellis Horwood, Chichester, UK.
Johnson, W., Sowerby, R. and Haddow, J. B. (1970) *Plane Strain Slip-line Fields: Theory and Bibliography*. Elsevier, New York.
Kachanov, L.M. (1974) *Fundamentals of the Theory of Plasticity*. Mir, Moscow.
Leroy, Y. and Ortiz, M. (1989) Finite element analysis of strain localization in frictional materials. *International Journal of Numerical and Analytical Methods in Geomechanics* **13**, 53–74.
Leroy, Y. and Ortiz, M. (1990) Finite element analysis of transient strain localization phenomena in frictional solids. *International Journal of Numerical and Analytical Methods in Geomechanics* **14**, 93–124.
Leroy, Y. and Triantafyllidis, N. (1996) Stability of a cohesive, frictional layer on a viscous substratum: Variational formulation and asymptotic solution. *Journal of Geophysical Research* **101**(B8), 17795–17811.
Lin, J. and Parmentier, E. M. (1990) A finite amplitude necking model of rifting in brittle lithosphere. *Journal of Geophysical Research* **95**(B4), 4909–4923.
Lockner, D. A. and Byerlee, J. D. (1993) How geometrical constraints contribute to the weakness of mature faults. *Nature* **363**, 250–252.
Mäkel, G. and Walters, J. (1993) Finite element analyses of thrust tectonics: computer simulation of detachment phase and development of thrust faults. *Tectonophysics* **226**, 167–185.
Mandel, J. (1966) Condition de stabilité et postulat de Drucker. *Proceedings of the Symposium on Rheology and Soil Mechanics*, pp. 58–68, Grenoble.
Mandl, G., Jong, N. J. and Maltha, A. (1977) Shear zones in granular material. *Rock Mechanics* **9**, 95–144.
Mandl, G. (1988) Mechanics of tectonic faulting: models and basic concepts. In *Developments in Structural Geology*, Vol. 1, ed. H. J. Zwart. Elsevier, Amsterdam.
Needleman, A. (1988) Material rate dependence and mesh sensitivity in localization problems. *Complementary Methods in Applied Mechanical Engineering* **67**, 69–86.
Odé, H. (1960) Faulting as a velocity discontinuity in plastic deformation. *Memoires of the Geological Society of America* **79**, 293–321.
Parsons, T. and Thompson, A. (1993) Does magmatism influence low angle faulting? *Geology* **21**, 247–250.
Pietruszak, S. and Mróz, M. (1981) Finite element analysis of deformation of strain-softening materials. *International Journal of Numerical Methods and Engineering* **17**, 327–334.
Poliakov, A. N. B. and Herrmann, H. J. (1994) Self-organized criticality in plastic shear bands. *Geophysics Research Letters* **21**, 2143–2146.
Poliakov, A., Hermann, H. J., Podladchikov, Y. and Roux, S. (1994) Fractal plastic shear bands. *Fractals* **2**, 567–581.
Pollard, D. D. and Segall, P. (1987) Theoretical displacements and stresses near fractures in rocks: applications to faults, joints, veins, dikes, and solution surfaces. In *Fracture Mechanics of Rocks*, ed. B. K. Atkinson, pp. 277–350. Academic Press, California.
Price, R. A. (1988) The mechanical paradox of large overthrusts. *Bulletin of the Geological Society of America* **100**, 1898–1908.
Regenauer-Lieb, K. (1996) Plastic velocity vector diagrams applied to indentation and transpression in the Alps. *Journal of Geodynamics* **21**, 339–353.
Regenauer-Lieb, K. and Petit, J.-P. (1997) Cutting of the European continental lithosphere: Plasticity theory applied to the present Alpine collision. *Journal of Geophysical Research* **102**(B4), 7731–7746.
Rudnicki, J. W. and Rice, J. R. (1975) Conditions for the localization of deformation in pressure-sensitive materials. *Journal of the Mechanics and Physics of Solids* **23**, 371–394.
Salençon, J. (1974) *Théorie de la Plasticité pour les Applications á la Mécanique des Sols*. Eyrolles, Paris.
Sanford, A. R. (1959) Analytical and experimental study of simple geologic structures. *Bulletin of the Geological Society of America* **70**, 19–52.
Sibson, R. H. (1994) Crustal stress, faulting, and fluid flow. *Geofluids: Origin, Migration and Evolution of Fluids in Sedimentary Basins*, pp. 15–28. Special Publications of the Geological Society of London **54**.
Sluys, L. J. and de Borst, R. (1991) Solution methods for localization in fracture mechanics. In *Fracture Processes in Concrete, Rock and Ceramics*, eds J. G. M. van Meir, J. G. Rots and A. Bakker, pp. 661–671. E. & F.N. Spon, London.
Spencer, J. E. and Chase, C. G. (1989) Role of crustal flexure in initiation of low-angle normal faults and implications for structural evolution of the basin and range province. *Journal of Geophysical Research* **94**, 1765–1775.
Stockmal, G. S. (1983) Modeling of large-scale accretionary wedge deformation. *Journal of Geophysical Research* **88**(B10), 8271–8287.
Tapponnier, P. and Molnar, P. (1976) Slip-line field theory and large-scale continental tectonics. *Nature* **264**, 319–324.
Terzaghi, K. (1943) *Theoretical Soil Mechanics*. Wiley, New York.
Timoshenko, S. and Woinowsky-Krieger, S. (1959) *Theory of Plates and Shells*. McGraw Hill, New York.
Turcotte, D. and Schubert, G. (1982) *Geodynamics, Applications of Continuum Physics to Geological Problems*. Wiley, New York.
Unger, D. J. (1995) *Analytical Fracture Mechanics*. Academic Press, New York.
Vardoulakis, I. (1980) Shear band inclination and shear modulus of sand in biaxial tests. *International Journal of Numerical and Analytical Methods in Geomechanics* **4**, 103–119.
Vardoulakis, I. and Graf, B. (1985) Calibration of constitutive models for granular materials using data from biaxial experiments. *Géotechnique* **35**, 103–119.
Vardoulakis, I. and Salem, J. (1995) *Bifurcation Analysis in Geomechanics*. Blackie Academic and Professional, Glasgow.
Vermeer, P. A. (1990) The orientation of shear bands in biaxial tests. *Géotechnique* **40**(2), 223–236.
Vermeer, P. A. and de Borst, R. (1984) Non-associated plasticity for soils, concrete and rocks. In *Heron*, ed. Stevin-laboratory of Civil Ingineering, University of Technology, Delft and Institute TNO for Building Materials and Building Structures, Rijswijk, The Netherlands, Vol. 29(3), pp. 1–75.
Wills, S. and Buck, W. R. (1997) Stress-field rotation and rooted detachment faults: a Coulomb failure analysis. *Journal of Geophysical Research* **102**, 20503–20514.

Yin, A. (1989) Origin of regional, rooted low-angle normal faults: a mechanical model and its tectonics implications. *Tectonics* **8**(3), 469–482.

Yin, A. (1993) Mechanics of wedge-shaped fault blocks 1. An 'elastic' solution for compressional wedges. *Journal of Geophysical Research* **98**(B8), 14245–14256.